Design and verification of a hermetic high-speed turbogenerator concept for biomass and waste heat recovery applications

Grönman Aki, Nerg Janne, Sikanen Eerik, Sillanpää Teemu, Nevaranta Niko, Scherman Eero, Uusitalo Antti, Uzhegov Nikita, Smirnov Alexander, Honkatukia Juha, Sallinen Petri, Jastrzebski Rafal, Heikkinen Janne, Backman Jari, Pyrhönen Juha, Pyrhönen Olli, Sopanen Jussi, Turunen-Saaresti Teemu

DOI: 10.1016/j.enconman.2020.113427

Design and verification of a hermetic high-speed turbogenerator concept for biomass and waste heat recovery applications

Aki Grönman[1], Janne Nerg[1,3], Eerik Sikanen[1], Teemu Sillanpää[1], Niko Nevaranta[1], Eero Scherman[2], Antti Uusitalo[1], Nikita Uzhegov[1], Alexander Smirnov[1], Juha Honkatukia[1], Petri Sallinen[1], Rafal P. Jastrzebski[1,3], Janne Heikkinen[1], Jari Backman[1], Juha Pyrhönen[1], Olli Pyrhönen[1,3], Jussi Sopanen[1], Teemu Turunen-Saaresti[1,3]

[1] *Lappeenranta-Lahti University of Technology, School of Energy Systems, P.O. Box 20, 53851 Lappeenranta, Finland*

[2] *LAB University of Applied Sciences, Yliopistonkatu 36, 53850 Lappeenranta, Finland*

[3] *Aument Power Oy, Lappeeranta, Finland*

Abstract

Many waste heat recovery and biomass applications offer opportunities for small-scale steam turbines to produce electricity and to improve systems energy efficiency. However, the currently used axial turbine-based technology is generally characterized by a relatively large physical size and poor design and off-design performances. To overcome these challenges, a new compact water-cooled high-speed radial outflow turbine concept is proposed. While the previous understanding of the chosen novel rotor water cooling approach indicates general system feasibility, improved turbine performance, and good potential, the scientific literature lacks relevant information. Since the design of high-speed machines is always case-dependent, every concept must be verified. Hence, to provide verification and new scientific information, this study combines analytical, numerical, and experimental analyses. The results predict turbine performance levels comparable with the previous radial outflow design, and its efficiency was found to exceed those of conventional turbines. During the experiments, the turbine also produced electricity from poor-quality steam, and its rotor dynamic behavior and magnetic bearing performance were close to the predicted results. These findings are considered a verification of the proposed concept. Furthermore, the rotor water cooling approach improved the stability of the system operation and although its physical behavior was not fully resolved, the study was able to verify its feasibility. In addition, at below 200 €/kW, the turbogenerator costs are competitive against competing technologies.

Email address: *Corresponding author: Tel. +358 40 776 7999 gronman@lut.fi (Aki Grönman[1])

Keywords: Steam turbine, radial outflow turbine, high-speed generator, active magnetic bearings, waste heat recovery, biomass

---

Nomenclature

Latin alphabet

c_x	axial chord	mm
h	specific enthalpy	kJ/kg
H	height	mm
M_2	vane outlet Mach number	-
N	number of vanes/blades	-
N_s	specific speed	-
p	number of pole pairs	-
p	static pressure	Pa, Bar
p_t	total pressure	Pa
P	power	kW
$q_{v,out}$	volume flow at turbine outlet	m^3/s
q_m	mass flow	kg/s
Q_s	number of stator slots	-
Q_r	number of rotor bars	-
R	degree of reaction	-
T	temperature	K, °C
Y	total pressure loss coefficient	-

Greek alphabet

η	efficiency	-
ϕ	heat power	kW
ω	angular speed	rad/s

Subscripts

el	electric
in	inlet
min	minimum
out	outlet
s	isentropic
turb	turbine

Abbreviations

AMB	active magnetic bearing
CFD	computational fluid dynamics
CHP	combined heat and power
DE	drive end
FE	finite element
FEM	finite element method
IM	induction machine
MIMO	multi-input multi-output
NDE	non-drive end
ORC	organic Rankine cycle
PEEK	polyether ether ketone
PMSM	permanent magnet synchronous machine
ROT	radial outflow turbine
TG	turbogenerator
UMP	unbalanced magnetic pull

1. Introduction

The small-scale Rankine cycle has been identified as a suitable method to improve the system energy efficiency of various applications. Larsen et al. [1] found that a 5% improvement in ship energy production can be achieved with a steam cycle. An efficiency increase of up to 3.5% was reported by Livanos et al. [2] for an LNG ship when using a steam turbine. The study by Uusitalo et al. [3] showed that for the studied cruise ships, an efficiency improvement of around

1-1.5% of the ships energy production was achievable. The best performance was predicted for a sub atmospheric pressure steam turbine or a combination of an atmospheric steam turbine and an organic Rankine cycle (ORC) process. In a review by Lion et al. [4], engine efficiency improvements due to a steam turbine recovering waste heat were in the order of 5%.

In biomass powerplants, there are also several cases where a small-scale steam turbine with a power below a few megawatts can be a feasible choice for electricity generation. For example, in a sawmill, biomass by-products can be used to produce steam that is further converted into electricity by these turbines, as discussed by Leino et al. [5]. Also, in some powerplants, there is excess steam available when the produced steam is not being used by consumers. In these situations, a boiler shutdown is not reasonable for a short period of time, and thus a small-scale steam turbine is a good option to produce electricity from the available steam. In addition, more advanced biomass-related energy generation processes can also offer opportunities, as was modeled by Ghaffarpour et al. [6] with an integrated gas turbine-solid oxide fuel cell-steam turbine cycle.

Especially in biomass applications, organic Rankine cycles have been preferred in recent years [7], and they can be considered as the main competing technology. Compared to ORCs, the main benefits of small-scale steam turbines are that water can be used instead of organic fluid, the use of a thermal oil circle can be avoided, and water can be exposed to high temperatures without the risk of decomposition. In addition, if industrial excess steam is used for power production, steam turbines are capable of directly utilizing the steam flow, whereas an ORC requires the installation of a full power system. As a result, small-scale steam turbines are easier to assemble, and the physical size of the system is smaller. The latter is especially important in marine applications, but it can also offer a clear benefit in many retrofitting cases. However, the efficiency and off-design performance of these turbines tend to be relatively poor because of high work impulse designs. Currently, the largest turbine manufacturers generally offer either single- or multi-stage axial turbines at power levels below a few megawatts, typically with a reduction gearbox and impulse

blades; this is considered as the industry standard. It is also worth mentioning that magnetic bearings are not currently used in steam turbines. For example, in the power range below 2 MW, Mitsubishi Heavy Industries [8] offers only multi-stage impulse designs with a reduction gearbox. Similarly, Siemens [9] has only single-stage impulse designs with either ball, sleeve or tilting pad bearings in their below 2.5 MW steam turbine portfolio.

A radial outflow turbine (ROT) is one design option that can overcome both the efficiency and the off-design performance challenges of axial turbines. In comparison to axial turbines, ROTs are characterized by lower Mach numbers, and they can handle higher volume flows, as was discussed by Persico et al. [10]. Furthermore, the opportunity to have a small inlet radius in the first stage helps to avoid partial admission-related aerodynamic losses. These benefits partly explain the higher aerodynamic efficiency. Luo et al. [11] predicted a total to static isentropic efficiency above 90% with improved off-design performance compared to axial turbines. According to Welch and Boyle [12], with single-stage ROTs, the isentropic efficiency can reach values above 80%, while conventional steam turbines of comparable power may even operate at isentropic efficiencies below 50%. In addition, Martin and Kolenc [13] presented experimental multi-stage ROT efficiencies from 60% to 90% in the power range of 8 kW to 1100 kW. These benefits have increased the interest in ROTs in the ORC industry. A study by Zanellato et al. [14] presented experimental performance data and suggested that turbine efficiencies above even 90% could be achieved with a few megawatt ORC ROTs. In their work, Song et al. [15] predicted an efficiency of over 85% for a three-stage ROT. It should be noted, however, that at the micro ORC power level (below a few tens of kW), an axial turbine may have a higher efficiency than an ROT, as was predicted in the work of Al Jubori et al. [16].

Turbomachines based on high-speed technology are compact in size, and their rotational speeds are typically above 10 000 rpm. The turbomachinery parts, which have a high rotational speed, and the generator are coupled on the same shaft, and there is no gearbox; instead, a frequency converter is used to feed the electricity to the grid. The described technology is suitable for

various applications, such as the inverse Brayton cycle as shown by Di Battista et al. [17]. Grönman et al. [18] utilized high-speed technology in electric turbocharging, and a similar approach was later presented by Zhao et al. [19]. In gas turbines, for example, Renzi et al. [20] used this technology in a micro turbine, and Caposciutti et al. [21] took a similar approach. ORCs based on high-speed technology are often hermetic, and they can use the working fluid for bearing lubrication, as presented by, e.g., Larjola [22] and Turunen-Saaresti et al. [23]. In some applications, such as aeration compressors [24], active magnetic bearings (AMBs) are also employed.

As was presented above, several studies discuss the benefits of ROTs. In addition, AMB-based high-speed technology is used in various energy conversion applications. The design principles of the whole machine are typically presented at a superficial level or in separate studies that easily hide the connections between different components. However, the design process is always iterative, whereby different design areas are interconnected and several compromises have to be made in terms of component efficiency. Uzhegov et al. [25] studied a two-stage high-speed compressor with two different electric machine designs and showed, for example, how cooling, rotor dynamics, and manufacturing constraints affect the design. Smirnov et al. [26] highlighted that mechanical requirements can also affect the design process of a high-speed machine. From the perspective of the design process, the most important areas in high-speed technology based turbomachinery are process design, layout design, axial thrust compensation, machine cooling, bearing design, turbomachinery and generator design, leakage management, component integration, mechanical design, and rotor dynamics. It is also worth mentioning that the cost of the machine is an important constraint that can lead to various design compromises. As was pointed out by Uzhegov et al. [25], high-speed electric machine design is, in general, case-sensitive and each application has its own design limitations. This principle can be also extended to the whole high-speed system, including the turbo parts. Therefore, without experimental verification, it is not certain that a new system will work properly, even though its components are designed ac-

cording to known design principles and all limitations are taken into account.

Of the various design requirements, heat transfer management is probably the single most important. A poor cooling design can, for example, lead to challenges related to thermal expansion or overheating of the electric machine. Liquid cooling offers improved heat transfer over air, as is discussed, for example, by Chung and Kim [27] for battery applications. When applied to a high-speed rotating shaft, its effects on rotor imbalance, cooling, and thermal expansion are currently unknown. To the authors' knowledge, the public literature has not previously reported rotor cooling by water in a large-scale high-speed turbomachine application. However, Gerstler et al. [28] proposed an internal water-cooling scheme for a 30 kW 14,000 rpm high-speed electrical machine. While the research was only numerical, it was concluded that by optimizing the water flow channels, the total pressure drop and churning losses could be minimized.

Based on the presented background, it can be concluded that there is a general lack of scientific knowledge about high-speed technology based radial outflow turbines in the literature, both at the system and component levels. Based on the available information, it is expected that the use of radial outflow turbines can lead to higher turbine efficiency levels than conventional small-scale steam turbines. There is also a clear need to experimentally verify any new high-speed technology based turbomachinery concept due to their case sensitivity. Further, it is expected that the machine can operate as designed if the integration between the different components is done properly. It was also shown that the rotor shaft cooling is one of the key elements of the design process and that there is currently no scientific knowledge available about the performance and flow phenomena related to rotor water cooling in large-scale high-speed turbomachinery. It is, however, expected that water cooling is feasible with a successful design approach. To fill these research gaps, this study presents a detailed design and verification of a new hermetic oil-free high-speed radial outflow steam turbine concept that has a water-cooled rotor shaft, magnetic bearings, and an induction-type electric generator. The new concept also seeks

to push the industry state of the art one step further. The key novelties are outlined in the following:

- The performance of a new double flow radial outflow steam turbine is predicted.
- The new steam turbine concept is experimentally verified.
- The feasibility and performance of the new rotor water cooling approach are numerically and experimentally studied.
- The costs of the machine are estimated.

The paper is organized as follows: First, the process design is explained. This is followed by the sections explaining the design of the turbogenerator in detail, including the layout and assembly as well as the turbine, generator, and bearing design and the predictions for the turbine and generator efficiencies. Further, the mechanical design and heat transfer are outlined through the inclusion of the modeling results. After this, the experimental setup is presented. The experimental results are provided in the next section, which also examines the specific features of the rotor cooling, estimates the cost level of the turbogenerator, and compares these with competing technologies. Finally, the conclusion is drawn.

2. Process Design

The turbine was designed for 330 ^{o}C and 10 bar steam inlet conditions based on measured data of steam properties in an actual small-scale biomass power plant producing process heat for industrial processes. In this application, the turbine is directly connected to the boiler. The turbine is designed for the 1 bar(a) outlet pressure in order to avoid vacuum conditions at the turbine outlet. This design choice also allows to keep the expansion above the saturation line, which helps to avoid droplet erosion in the last turbine stages. In addition, the relatively high temperature in the condenser allows to use the condenser heat

for heating purposes in CHP applications. The turbogenerator design values are presented in Table 1.

The steam values are also close to the steam values of large-scale engine combined cycle power plants [29] and the steam values in modern ships equipped with steam boilers for producing steam from the heat of the main engines [30]. Thus, the choice of the design conditions matches several applications. Fig. 1 presents a simplified example of the turbogenerator installed in a indirect hermetic connection in a combined cycle power plant. In this application, the electric efficiency of the steam cycle is approximately 13%. However, higher efficiencies are achievable if lower condensing pressures and temperatures are utilized. The electric efficiency is defined as

$$\eta_{\mathrm{el}} = \frac{P_{el}}{\phi}. \tag{1}$$

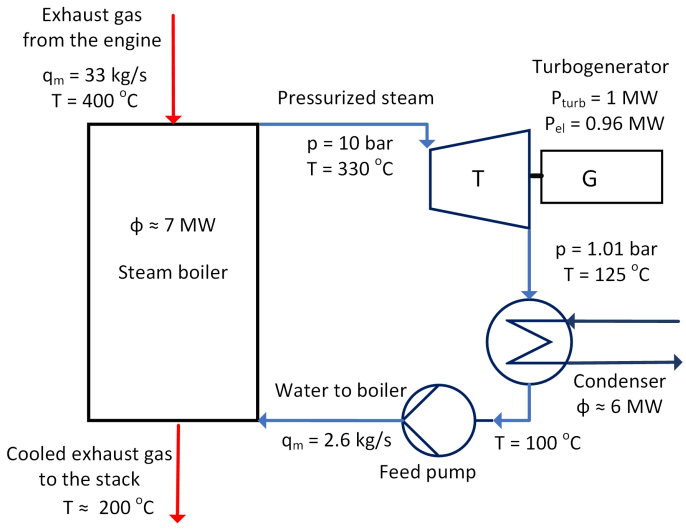

Figure 1: Simplified example of a 1 MW steam turbine cycle installed for recovering exhaust gas heat of large-scale reciprocating engines.

Table 1: Turbogenerator design values.

Steam inlet temperature	330 ^{o}C
Steam inlet pressure	10 bar
Steam flow rate	2.44 kg/s
Turbine outlet pressure	1 bar
Rotational speed	208 Hz
Electric power	1000 kW
Turbine isentropic efficiency	80 %

3. Turbogenerator Design

First, the layout and assembly of the turbogenerator are presented, and second, the design of each main component is described in detail to provide an in-depth analysis of the design principles.

3.1. Layout and assembly

The turbogenerator (TG) consists of two main parts; the electric machine and the turbine. A cross-sectional view of the TG is shown in Fig. 2. The electric machine is an induction generator with a nominal power of one megawatt. The rotor type is a solid-state squirrel cage rotor with 20 embedded copper bars and internal cooling channels in the rotor. The copper bars are attached to the copper end rings by expanding the diameter of the copper bar at the joint. The copper bar diameter is enlarged by inserting an oversized pin inside the end of the copper bar. Even though a special high-strength copper alloy is used, the copper end rings must be supported by stainless steel sleeves to sustain the centrifugal loads caused by high rotational speeds. The cooling channels are located under the copper bars. The cooling water is fed in at the non-drive end (NDE) of the rotor, as is also seen in Fig. 7, and the cooling water exits from the drive end (DE), and the cooling channels are connected to the steam

outlet. For easier manufacturing of the drilled long holes for rotor cooling, the prototype rotor is a two-piece construction with a shrink fit between the two rotor halves.

The rotor is supported by active magnetic bearings. The radial bearing stators are sealed inside a can in order to protect the AMB stators from the water and steam from the process. The radial AMBs are connected to the bearing plates at both ends of the frame tube. The axial AMB stators are not sealed inside the can. Located in the upper end of the machine, the axial AMB stator is partly water cooled. This is due the fact that any excess cooling water from the rotor water cooling input system will be collected on top of the axial AMB stator. The overflowing water is drained through the frame. The AMB system is backed up by mechanical touchdown bearings (ball bearings).

The frame of the induction generator consists of a supporting frame structure and the electrical machine stator. The stator is cooled by direct water-cooled stator coils with a water insulation system inside the electrical coil. All connections, inlets, and outlets are sealed in order to create a hermetic system. To achieve a hermetic system, the sealing design is important. The variety of the seals used include O-rings, flange seals, compression packings, and also labyrinth seals.

The turbine impeller is directly attached to the end of the induction generator rotor. The turbine housing includes cast turbine casings and machined turbine stator blades. As each part of the assembly is subjected to corrosion by hot steam and water, the material selection is critical. All parts that may corrode are made of noncorrosive materials. The steam is fed into the turbine from eight positions that are located 90 degrees from each other. They are also symmetrical at the upper and lower sides of the double-flow turbine.

3.2. Turbine design

Typically, the type of a turbine is chosen based on a Cordier diagram, where the specific speed N_s is used to determine the turbine type

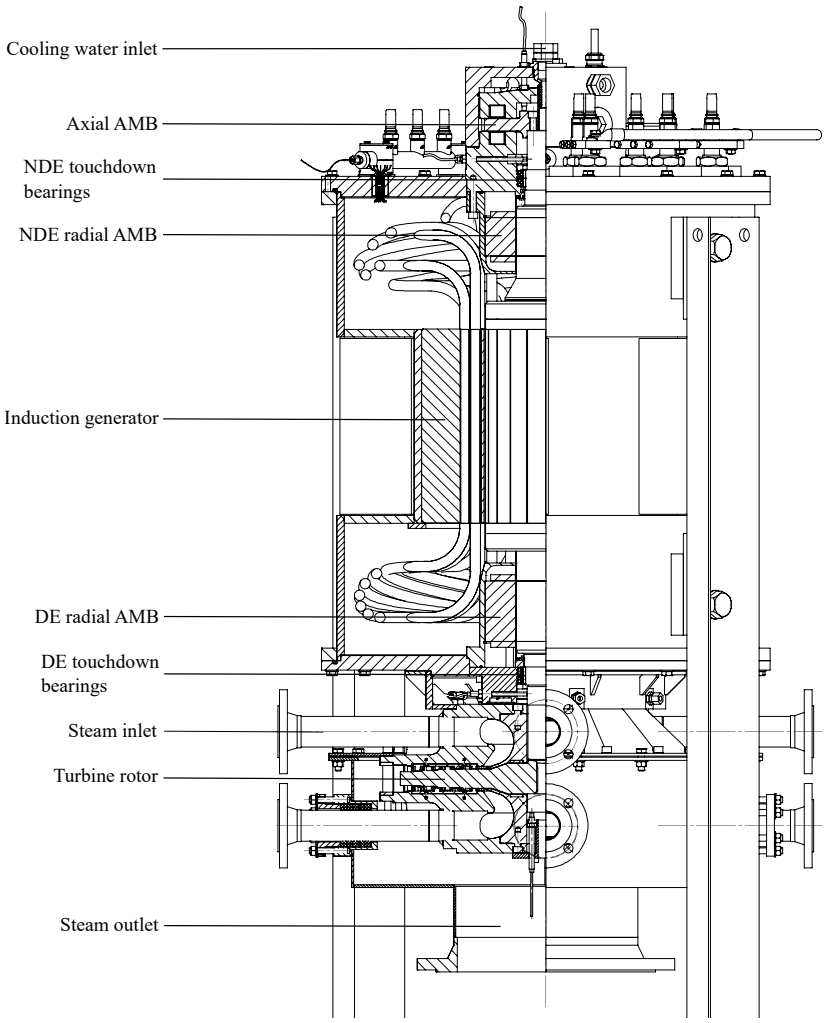

Figure 2: Cross-sectional view of the turbogenerator.

$$N_{\mathrm{s}} = \frac{\omega\sqrt{q_{v,out}}}{\Delta h_s^{3/4}}. \tag{2}$$

At specific speeds less than unity, a radial turbine is usually chosen; when above 2, an axial turbine is used, and between these values, a mixed flow turbine has the best performance. When working with specific speeds less than 0.1, according to Balje [31], partial admission turbines have a higher efficiency potential than full admission ones. For the current design, the specific speed

is 0.1, which means that typically, a supersonic single-stage partial admission turbine would be chosen for the application. However, this would mean a poor off-design performance, but on the other hand, there would be no axial force to be compensated. To overcome the off-design challenge, it is proposed that a radial outflow turbine could offer subsonic expansion with good off-design characteristics but also with a short axial length. In order to compensate the axial thrust, the ROT was designed as a symmetrical double-flow layout, shown in Fig. 2, and to the authors' knowledge, it is the first of its kind.

A turbine design tool was developed to allow a fast preliminary design of a ROT with a variable number of stages. In the first design phase, the turbine stage performance is estimated by Soderberg's loss correlation for axial turbines [32]. It is a simple loss prediction method for turbine cascades, which can be used to give performance estimations in the early design phase. It was also built on steam turbine and cascade data and was further extended to very small aspect ratios, making it attractive for the current design. The design tool delivers all information required to compare different designs and check if the limiting design factors are acceptable. As a result of this part, for instance blade heights, radii, chords, and flow angles are obtained. The suitability of Soderberg's loss correlation for a ROT at aspect ratios that are valid for the designed turbine is evaluated in Fig. 3. The total pressure loss coefficient of a turbine blade is defined as

$$Y = \frac{p_{t,in} - p_{t,out}}{p_{t,out} - p_{out}}, \tag{3}$$

and it is compared with the numerical simulations by Grönman et al. [33] at different aspect ratios. The results predict acceptable trends between the methods, although Soderberg's method overestimates the losses. The observed trend means that the design tool is expected to predict conservative performance values when compared with numerical simulation.

The limiting design factors in the evaluation of the suitability of the radial outflow turbine design are the minimum blade height and the opening angle of

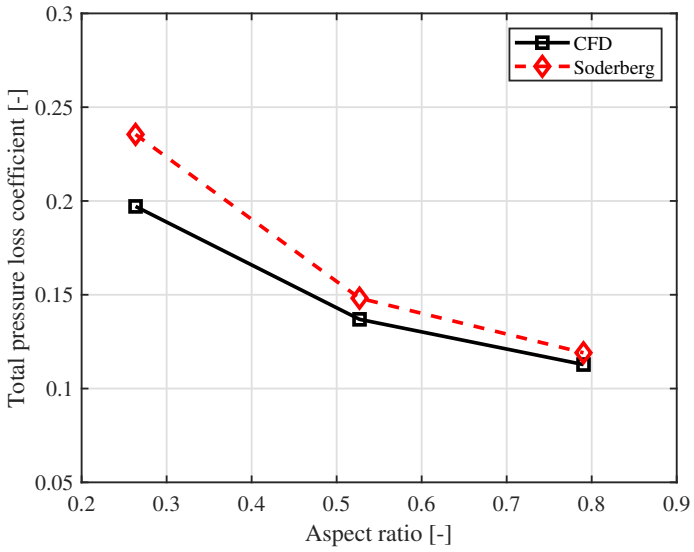

Figure 3: Total pressure losses of turbine blades at different aspect ratios (H/c_x). A comparison between a numerical simulation by Grönman et al. [33] and Soderberg's loss correlation [32].

the flow passage. A value of 2 mm was used as a minimum acceptable blade height. This limit is based on in-house manufacturing experiences. Furthermore, the flow passage opening angle should not exceed 30^o in order to limit the endwall boundary layer separation [10]. Additionally, from the perspective of efficiency, it is beneficial that the flow remains subsonic as the presence of shock waves may degrade the efficiency.

The design, in general, follows the typical axial turbine design path except that the radius is not constant along the meanline. Despite this difference, axial turbine loss correlations have been used with a good accuracy in radial outward flow ORC turbines. Pini et al. [34] successfully employed axial turbine correlations in an ORC turbine design process. Persico et al. [10] compared numerical simulations with axial turbine loss correlations and found slight profile loss over prediction by the correlations. Partly similar findings were also made later by Grönman et al. [33]. In the current work, the design of each turbine blade row was also verified with a 2D CFD simulation, where the velocity triangles and the

Table 2: Turbine design parameters.

	Vane 1	Blade 1	Vane 2	Blade 2	Vane 3	Blade 3	Vane 4	Blade 4
R [-]	-	0.25	-	0.25	-	0.25	-	0.44
M_2 [-]	0.53	-	0.67	-	0.84	-	0.79	-
N [-]	80	81	87	83	97	89	103	95
P [kW]		70.6		109.5		156.6		161.6
H/c_x [-]	0.42	0.32	0.38	0.32	0.55	0.43	0.72	0.73
H_{min} [mm]	4.3	4.5	4.3	5.1	5.1	7.0	7.8	9.8

expansion processes were compared with the ones obtained from the 1D design tool.

After several iterations, it was found that for the given input values, a four-stage turbine results in a geometry that allows a smooth expansion between each blade row and results in acceptable blade heights but also keeps the Mach numbers subsonic, as seen in Fig. 4 and Table 2. The first three turbine stages have a constant degree of reaction in order to get more power from a stage while maintaining reasonable off-design operation. The degree of reaction of the last stage is, however, higher in order to reach the target outlet pressure.

It is clearly visible in Table 2 that the power increases from the first stages until the maximum power is found in the last stage. Because the turbine consists of two symmetrical sides, the powers are predicted for the other half only. The expected power of the turbine is 997 kW with a total-to-static isentropic efficiency of 83.5%, which is high compared with typical single-stage supersonic axial turbine designs. This design is also well in line with the turbine performance of the process design values presented in Table 1.

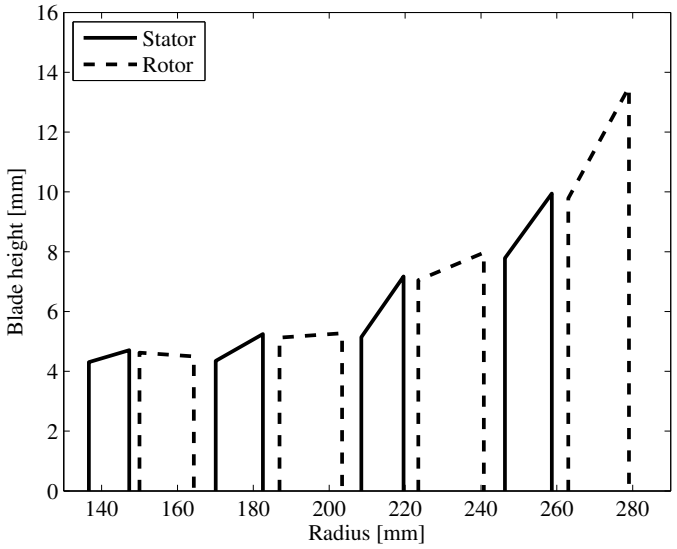

Figure 4: Two-dimensional side view of the radial outflow turbine geometry.

3.3. Generator design

The generator design was based on the constraints set by the turbine design, that is, the generator rotational speed, nominal power, and thereby nominal torque were fixed to match the corresponding values of the turbine. As the design turbine output power is 1 MW at the rotational speed of 208 Hz, a high-speed electric machine acting as a generator is needed to reach a compact solution, where the turbine and the generator are mounted on the same shaft in order to avoid a step-down mechanical gear. This also has a positive impact on the overall efficiency of the mechanical drivetrain, because the losses caused by the mechanical gear are avoided. Furthermore, the speed control of the mechanical drivetrain can be accomplished by a generator frequency converter. To maximize the overall efficiency, the target value of the electrical efficiency of the generator was set to be more than 96%.

There were two alternatives for the generator type; an induction machine (IM) and a permanent magnet synchronous machine (PMSM), both of which are widely used in high-speed applications [35]. The major limitation regarding

the electrical machine type selection is related to the hermetic structure of the turbogenerator, because it has a significant impact on the cooling solution and the material selection. First of all, a hermetic structure does not allow the use of open circuit forced air cooling, and secondly, because of the leakage steam from the turbine, all the materials used in the electrical machine must tolerate humidity [36]. Even though a PMSM has a higher electrical efficiency than an IM, permanent magnets are very vulnerable to high temperatures [37]. Furthermore, a mechanical structure preventing leakage steam from coming into contact with permanent magnets will result in a complex and expensive rotor structure. Therefore, an induction machine with a solid iron rotor and a copper squirrel cage was selected as a generator topology.

The selection of the number of magnetic poles has an impact on the generator performance and the axial length of the generator active parts. The number of magnetic poles affects both the magnetizing inductance and the output frequency of the generator inverter. Magnetizing inductance is inversely proportional to the number of pole pairs, and thus, increasing the pole pair number from one to two decreases the magnetizing inductance by 50% [38]. This leads to a lower power factor, and therefore, the generator inverter must be overrated to provide the reactive power needed to magnetize the machine. At the same time, the output frequency of the generator is doubled, which increases the inverter and iron losses of the generator. The benefit of using the pole pair number $p > 1$ is that the axial length and the total space needed by the end windings are considerably smaller than in the case of $p = 1$. In the design process, it was concluded that in the studied case, it is more profitable to minimize the overrating of the inverter while maximizing the electrical efficiency of the generator by selecting a structure with $p = 1$. The number of stator slots is $Q_{\mathrm{s}} = 18$, and the number of rotor bars is $Q_{\mathrm{r}} = 20$. The stator winding is a conventional double-layer winding. Because the solid rotor acts as a solid current path, it is extremely important to minimize the rotor surface losses [39]. This is done by using an air gap of 5 mm, cutting the eddy current path by opening the iron bridge above the rotor bars, and extending the semimagnetic stator slot wedges

Table 3: Main parameters of the induction generator.

Parameter	Value
Total stack length [mm]	380
Rotor length [mm]	420
Stator inner diameter [mm]	247
Stator outer diameter [mm]	487
Rotor outer diameter [mm]	237
Rotor tangential tension at rated torque [kPa]	22
Number of stator slots [-]	18
Number of rotor bars [-]	20
Effective coil turns in half-slot [-]	1
Stator coil turns per phase [-]	6
Winding factor [-]	0.902
Number of pole pairs [-]	1
Number of slots per pole and phase [-]	3

slightly into the air gap. Air gap flux density harmonics are further reduced by employing 7/9 short pitching in the stator winding. Short pitching also helps to minimize the axial length of the end windings. The main parameters of the generator are provided in Table 3.

The hermetic structure of the cooling system of the generator comprises directly water-cooled stator core windings and a water-cooled rotor structure. The direct water cooling of the stator windings is achieved by using a construction where a brass tube acting as a cooling channel is placed at a center of the copper conductors. One coil conductor comprises 90 parallel-connected polyether ether ketone (PEEK) insulated copper conductors. The outer diameter of one conductor including the PEEK insulation layer is 1.66 mm. The parallel-connected wires are wound around a brass tube, the outer diameter of which is 6.35 mm

Table 4: Operational data of the generator.

Parameter	Value
Rated speed [Hz]	208
Rated voltage [V]	675
Rated electric power [kW]	1000
Rated torque [Nm]	766
Rated stator current [A]	1170
Power factor cos ϕ in the rated operating point [-]	0.80
Rated point efficiency [%]	96.42

and the wall thickness 0.89 mm. The brass tube is insulated with PEEK heat shrink tubing. The copper conductors are twisted around the brass tube to avoid eddy-current losses. The rotor is made of ferromagnetic stainless steel EN 1.4021, and the rotor structure is hollow so that the cooling water flows through the rotor to the condenser. The operational data of the designed generator are given in Table 4, which predicts that the targeted performance can be achieved.

3.4. Bearing design

The selection of active magnetic bearings for the design results from the high rotational speed and the presence of steam. In such a harsh environment, traditional ball bearings do not survive long enough, oil bearings are not suitable because of the steam, and water bearings will result in significantly higher losses. The AMBs provide levitation with a magnetic field, thereby eliminating the contact between the moving parts. Thus, only air friction is present and there is no wear of components, which significantly reduces the need for maintenance.

The main criterion for the magnetic bearings are the forces they need to provide. They can be estimated when the mass of the rotor and the system arrangement are known. The generator is placed in a vertical position, and

therefore, the axial bearing should compensate most of the gravitational force. However, as the system is designed with one of the possible applications being intended for marine use, it should be able to handle an inclination angle of 22.5^o. Thus, in the worst case, the radial bearings should tolerate around 35% of the total mass. The bearing near the turbine impeller is intentionally designed larger to improve the controllability at the heavier end. The smaller radial bearing is adjusted to take 35% of the total force, the larger one taking 65%.

In addition to the gravity forces, the radial bearings should tolerate other forces in the system, such as unbalance force [40]. This force is estimated based on the maximum rotational speed and the balancing level. For the system in question, a balancing grade of G2.5 was selected to obtain a machine structure that would satisfy the criteria of vibration limits given for AMB-supported high speed machines [41]. Furthermore, a safety factor of two was introduced to overcome tolerances, manufacturing imperfections, and errors in the modeling process.

With the force requirements known, the structure of the bearing was selected. For the topology, a heteropolar E-core design was adopted. The rotational speed of 208 Hz is not too high to use a homopolar bearing, but heteropolar ones are easier from the perspective of manufacturing [42]. The E-core pole arrangement provides flux splitting and thereby reduces the lamination thickness on the shaft and makes the rotor more rigid.

To isolate the coils of the magnetic bearings from the process, a canned solution presented in Fig. 5 was used. Thus, the magnetic air gap was selected to be 1.15 mm, the can taking 0.8 mm of that space, and the rest being left for the mechanical gap where the rotor can move. The thickness of the can is defined by the mechanical properties, and the can should be strong enough to withstand the process pressure. Because of the large magnetic gap, considerable space is reserved for the coils to achieve the necessary current linkage. The radial bearings are designed to operate close to the BH curve knee of 1.2 T. The main parameters of the bearings are presented in Tables 5 and 6.

A wide enough bandwidth is important for the radial AMB, and lamination

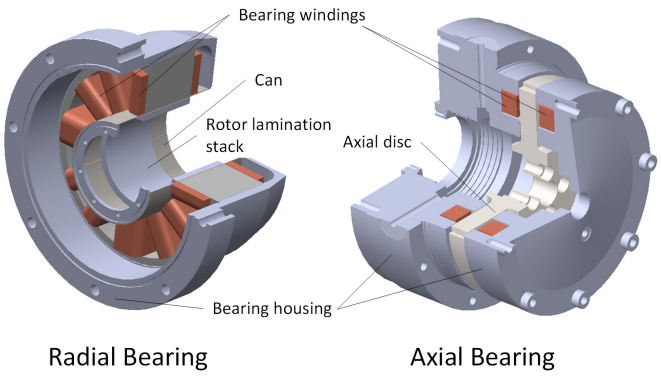

Figure 5: Schematics of the designed radial and axial magnetic bearings.

is used to avoid eddy currents [25]. For the stacks, the M270-35A lamination sheets were selected. They form the path for the magnetic flux in the stator and the rotor. For the can that separates the electromagnetic part from the process, the stainless steel EN 1.4301 was chosen as a cost effective material with corrosion resistance. This material is conductive and thus introduces eddy currents; however, the effect was considered insignificant. A phase lag less than 5^o was added at the nominal rotational frequency.

Touchdown bearings were applied in order to back up the AMBs in case of a failure in the AMB system by preventing the rotor–stator contact and allowing the rotor to drop on the touchdown bearings for safe machine shutdown. Angular ball bearing pairs of the bearing type XC 71916E T2RSDP4S UL were mounted in an X-arrangement next to the radial AMBs on both ends of the rotor. The lower touchdown bearing pair at the drive end can carry the loads in both the radial and axial directions, whereas the upper bearing pair in the non-drive end acts only in the radial direction.

3.5. Rotor cooling

The rotor of the turbogenerator is water cooled, provided with cooling channels as shown in Fig. 6. The cooling water inlet duct is equipped with a contactless labyrinth seal (Fig. 7) in order to minimize leakages at the non-drive

Table 5: Main parameters of the radial magnetic bearings.

Parameter	Value
Number of poles	12
Lamination material	M270-35A
Number of coil turns for a large pole	85
Number of coil turns for a small pole	54
Smaller Bearing	
Current stiffness [N/A]	170
Position stiffness [N/μm]	1.19
Maximum achieved force [N]	1110
Larger Bearing	
Current stiffness [N/A]	270
Position stiffness [N/μm]	1.88
Maximum achieved force [N]	1760

end of the rotor. Cooling water is fed into the rotor from the non-drive end. In the upper part of the rotor, the cooling water flows through a single circular flow channel at the center of the rotor. In the generator active part, the cooling water is split into ten cooling channels (radial outward, axial at the generator active length, and radial inward at the bottom of the generator). After the generator part, the cooling water is collected into a single circular cooling channel. The cooling water exits to the condenser at the bottom of the shaft (drive-end).

3.6. Mechanical design and heat transfer

This subsection is divided into three topics. First, the results of the thermal and stress analyses are presented for the turbine impeller; second, the rotor dynamic behavior of the rotor is analyzed. In addition, the control approach of the AMBs is explained.

Table 6: Main parameters of the axial magnetic bearings.

Parameter	Value
Number of poles	2
Material	X20Cr13
Number of coil turns	65
Current stiffness [N/A]	581
Position stiffness [N/μm]	5.68
Maximum achieved force [kN]	6.36

3.6.1. Turbine impeller temperature and stress distributions

In normal operation, the temperature distribution of the solid construction turbine impeller is mainly affected by the hot steam flows in the turbine blade cascades and on the surfaces of the impeller, as well as by the rotor cooling water flow. There are also steam leakage flows caused by the clearances between the rotating and stationary parts at the hub of the impeller, having an influence on its temperature distribution.

In this design procedure, the thermal analysis is closely linked to the stress, strain, and deformation analyses of the turbine impeller. The thermal analysis was conducted using the Ansys software. Thus, the 3D temperature distribution was numerically solved based on the 3D thermal conduction analysis of the solid construction of the impeller and using boundary conditions for the surfaces exposed to steam and cooling water flows. Related to the connection between the impeller and the shaft, the contact resistances between the adjacent solid parts were also included in the thermal analysis.

In the steady-state thermal study, the thermal model consists of 26 thermal convection constraints describing the heat rate from the steam to the turbine body, three thermal resistances describing the heat conduction over the solid bodies, and one fixed temperature constraint describing the effective wa-

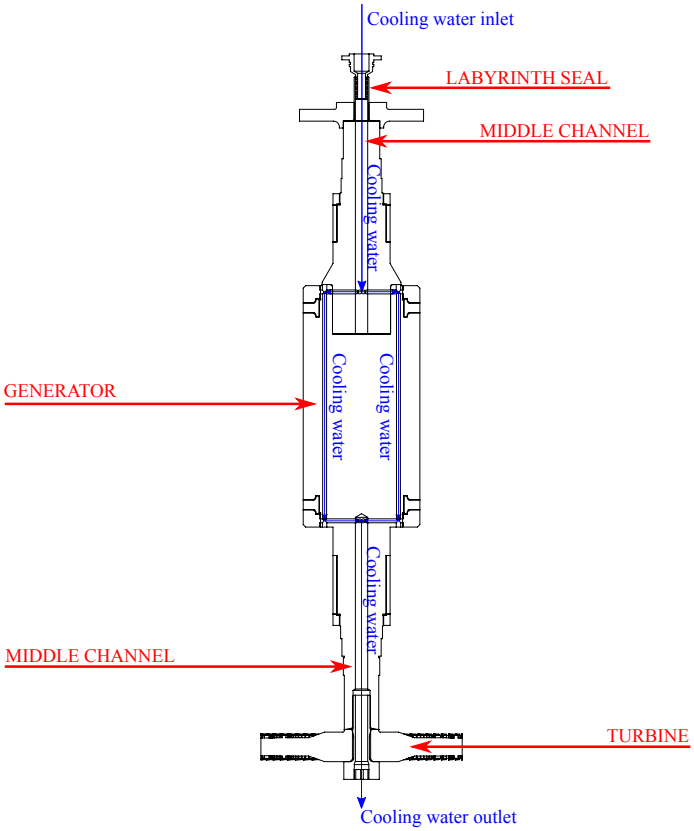

Figure 6: Water cooling paths in the rotor of the turbogenerator. The cooling water enters the rotor shaft from the non-drive end and is divided into ten cooling channels in the generator. Before exiting to the condenser, the cooling water is collected into a single channel after the generator.

ter cooling. In Fig. 8a, the high temperature at the hub is caused by the heat conduction from the hot sections of the solid impeller but also by the leakage flows between the turbine rotor and stator. Nonlinear thermal and mechanical material properties are used. Thus, also the material strength properties of the turbine impeller are nonlinear as a function of temperature.

In the static structural stress analysis performed with Ansys, the calculated 3D temperature distribution of the turbine impeller was used as an initial condition causing thermal expansion. The analysis was conducted for a normal

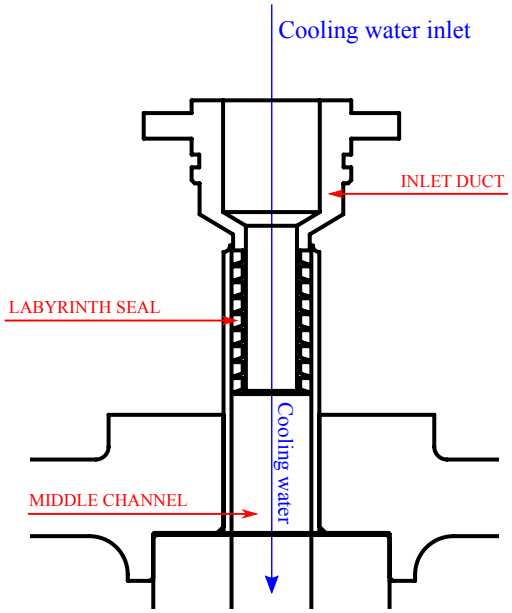

Figure 7: Labyrinth seal of the cooling water inlet duct at the upper end of the rotor.

water cooling situation where the impeller is cooled by the cooling water flowing in the middle channel of the shaft and through the impeller. The stress distribution of the situation under study is presented in Fig. 8b. A rotational speed of 208 Hz was used for the impeller and the shaft in the analysis. The stress results indicate that the safety factor (ratio between material strength and maximum stress) of the impeller is 1.34. The blade root stresses were also studied, although no significant stress levels were observed.

3.6.2. Rotor dynamics and AMB control

A finite element (FE) rotor dynamics model of the hermetic generator rotor was generated using Timoshenko beam elements. A total number of 46 beam elements was used. A varying mesh density was also used in order to increase the accuracy of the shear deformation effects between the geometrical changes in the rotor geometry. The axial AMB disk and the turbine impeller were modeled as rigid disks.

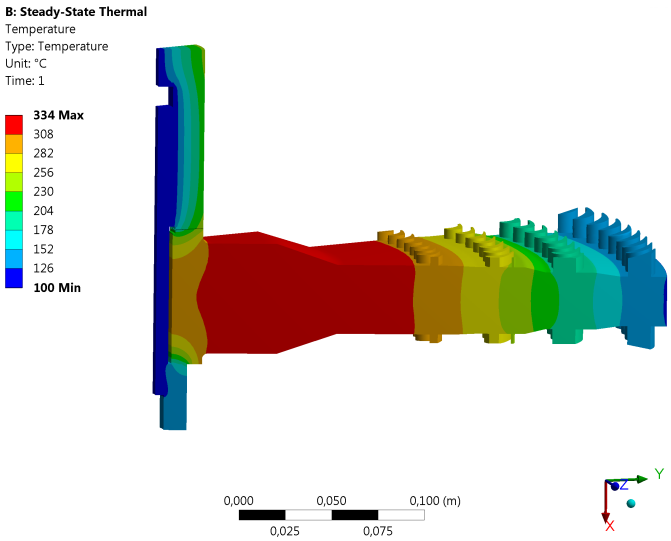

(a)

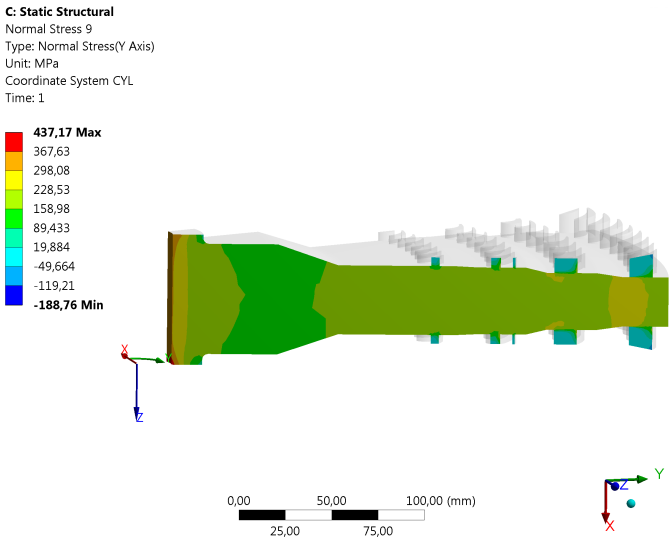

(b)

Figure 8: Modeled turbine impeller temperature (a) and stress distribution (b).

The generated FE model was verified by performing an experimental modal analysis for the manufactured rotor using laser vibrometer equipment. The

FE model was tuned to match the measured free body bending frequencies by modifying the material properties used. The first bending mode frequency of the FE model was set to exactly match the first measured bending mode frequency, although the second bending frequency in the FE model has a 12% margin of error. This is acceptable because the second bending mode frequency is significantly greater than the rotor spin frequency. The first two measured bending frequencies are 149 Hz and 324 Hz, respectively.

The generated Campbell diagram is presented in Fig. 13. The AMBs were modeled to be linear by using a stiffness coefficient of 1×10^6 N/m and a damping coefficient of 1×10^3 Ns/m. Based on the bearing model applied, the Campbell diagram indicates that the first backward critical speed occurs at 105 Hz and the first forward critical speed at 247 Hz. The estimated first forward mode is beyond the operational speed range with a 19% safety margin.

In addition to the rotor dynamic analysis, also the stator and frame structures were investigated. The FEM analysis indicated some resonance frequencies in the operational range for the original design. Therefore, some design changes were made to the end plates and the frame to increase the resonance frequencies above the operating speed range. This was crucial for the reliable AMB operation, because the AMBs are supported by the end plates and should have a rigid enough basis.

The AMB controller was implemented as a state space multi-input multi-output (MIMO) controller, which uses the rotor model as a basis for the plant model. Additionally, some filtering was added to the feedback signals to eliminate the resonance frequencies originated from the frame and piping structures.

4. Experimental Setup

The experiments were conducted at the Laboratory of Fluid Dynamics at LUT University. This paper presents the results from several different sets of measurements. In the first two sets of measurements, saturated steam was produced by two 2.5 MW steam trucks, and it was fed into the turbine through a

control valve. The steam was further divided into eight symmetric inlets into the turbine. Fig. 9 shows two of the turbine inlets and the connection to the main steam pipe. These measurements were conducted both with and without rotor cooling, and the target was to verify that the turbogenerator is mechanically feasible and can produce electricity, and the rotor cooling works as expected. In addition, verification of the machine dynamics and the AMB performance were important objectives of the measurements. Especially, the influence of the rotor coolant on the rotor balance was a topic of interest.

The steam mass flow was measured by a V-Cone with an estimated measurement accuracy of ±1%. One temperature measurement was installed before and after the turbine (K-type thermocouples), and two static pressures were measured before the turbine and one after the turbine by pressure tappings. The measurement errors for the temperatures were estimated to be ±1 K, and for the static pressures ±10 Pa. The rotational speed was measured from the AMB unit with an estimated accuracy of ±0.4 Hz. The generated power was measured after the inverter with a Yokogawa PZ-4000 power analyzer with an accuracy of ±0.1% of the reading. The rotor cooling water flow was also measured with a rotameter with an estimated accuracy of ±3%.

The position of the rotor was measured at ten different points by the differential measurement principle using eddy current sensors. There were four sensors for each radial bearing and two sensors for axial displacement. The lower radial AMB sensors were also water cooled, because they are located near the hot turbine housing.

During the experiments, the time-averaged steam conditions given in Table 7 were used. All the operating parameters in this work are averaged over 60 s with a 0.5 Hz recording frequency. It is pointed out that the turbine was operated in severe off-design conditions, which is considered acceptable from the perspective of the research objectives.

In the third set of measurements, the turbogenerator was rotated without a steam flow but with the rotor cooling on in various different conditions in order to better understand the fluid dynamic behavior of the cooling system.

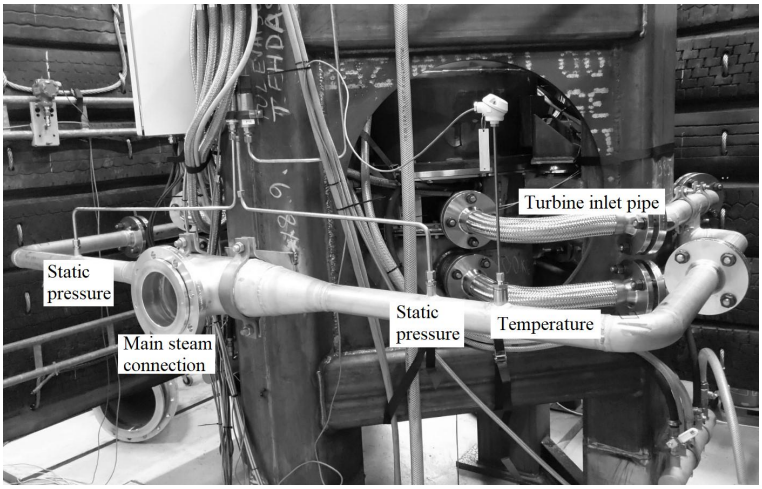

Figure 9: Turbine inlet piping and instrumentation.

An additional pressure measurement was also installed before the cooling water inlet.

5. Results and Discussion

This section first presents the results from the turbogenerator cost analysis. In the second part, the results from the laboratory experiments are analyzed to test the hypotheses and verify the design.

5.1. Cost of the turbogenerator

The costs of a machine are crucial when making investment decisions. Therefore, special attention was paid to materials and manufacturing in designing the prototype. These constraints led to several compromises between cost and performance. As a result, the total cost of the prototype materials, manufacturing, and assembly was 130 500 € (130.5 €/kW), and even lower costs in the range of 80 000–100 000 € can be expected when more turbogenerators are manufactured. It was also estimated that a 1 MW frequency converter costs

Table 7: Average steam parameters during the experiments.

Parameter	Value
Turbine inlet temperature [K]	409-416
Turbine inlet pressure [bar]	3.3-3.9
Steam mass flow [kg/s]	1.03-1.25
Turbine outlet pressure [bar]	1.0

approximately 60 000 €. As a result, the cost of the system is estimated to be below 200 €/kW. Compared with the conventional steam turbine cost estimates presented in Table 8, it can be seen that the cost of the proposed design is lower than the 350 €/kW and 636 €/kW range suggested by the literature. Even though a direct comparison with ORC powerplants is not straightforward, the realized turbogenerator price level (including the frequency converter) is competitive with the estimates by Lemmens [43] (see Table 8). In heat recovery applications, the lowest module prices are approximately 900 €/kW and the average cost is 2149 €/kW, while at the project level, the cost average is 3414 €/kW. Furthermore, the project cost in biomass applications is in the same order of magnitude as in heat recovery applications. It should, however, be mentioned that the lowest presented costs for biomass projects are in the range of 250–350 €/kW (power range 3–4 MW).

5.2. Experimental Results

Two sets of measurements with saturated inlet steam are presented here. The first set was performed without the rotor cooling, and in the second, a rotor cooling water flow of 5 l/s was used. Fig. 10 presents the performance of the turbogenerator during both measurements. The results show that the machine is capable of producing electricity even with low-pressure saturated steam and with mass flows that are 42–51% of the nominal value. The turbogenerator was

Table 8: Steam turbine and ORC cost estimates. The costs of steam turbines by Arsalis [44] and Ehyaei and Rosen [45] has been converted into Euro from US Dollars using 2020 rates.

Type	Power	Cost	Application	Reference
High-speed steam turbine	1 MW	<200 €/kW	Biomass, heat recovery	This work
ORC module (minimum)	5-6 MW	900 €/kW	Heat recovery	[43]
ORC project (minimum)	3-4 MW	250–350 €/kW	Biomass	[43]
Steam turbine	1 MW	350 €/kW	Triple cycle	[44]
Steam turbine	1 MW	636 €/kW	Triple cycle	[45]

not insulated during the measurements, and there were not enough accurate temperature measurements available. Therefore, the collected data cannot be used to evaluate the aerodynamic performance of the turbine.

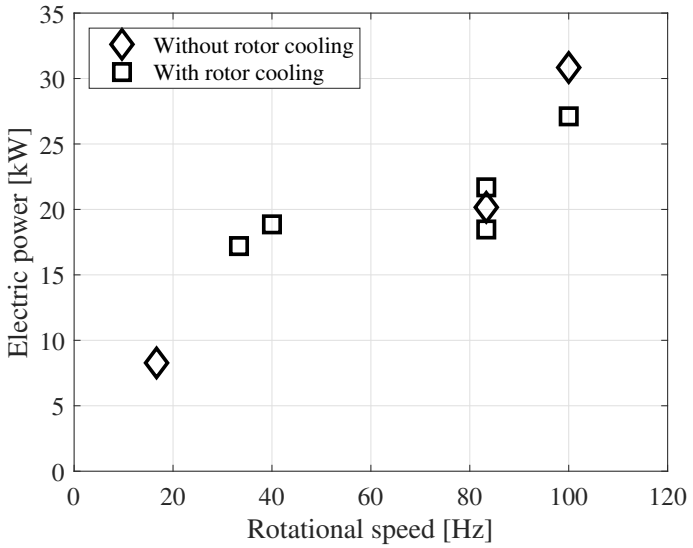

Figure 10: Turbogenerator performance with and without rotor cooling.

It is also noteworthy that without the rotor cooling, the turbine was operated at 133 Hz with low steam mass flow conditions. In this test, the turbogener-

ator was able to produce a peak electric power of 95 kW. However, the steam conditions did not settle, and therefore, average performance results are not presented here. Fig. 11 depicts this operating condition as an example of the transient performance of the turbogenerator. It shows that the electric power follows the changes of mass flow, although there is a time shift resulting from different measurement response times. This difference can also be seen Fig. 11b, which shows that there is a peak in the steam inlet temperature measurement at 24 s. This peak is also believed to be related to the measured 95 kW maximum power, and it gives an impression of the transient response of the system.

During the measurements, it was also noticed that without the rotor cooling, the axial clearance of the shaft became too small and caused problems. However, with the rotor cooling, the axial clearance problems disappeared and the turbogenerator operation remained comparable with the noncooled experiments. This finding is considered a proof of the performance of the rotor cooling design. The general operational characteristics of the rotor cooling are examined in the last set of measurements presented in Fig. 12. In the generator rotor, the cooling water flow is exposed to rotation of the rotor and gravitational effects. The line "Overflow limit" presents the limit above which the cooling flow is too high for the corresponding rotational speed, and a fraction of the cooling water is overflowing outside the cooling channel (overflow was detected visually). This phenomenon seems to have a correlation with the rotor rotational speed and with the cooling water volume flow rate; however, the physical phenomena remain unsolved. In addition, conclusions about the effects of the rotation of the rotor on the pressure drop of the cooling water flow cannot be made from the measured data. However, there is possibly a very weak trend between the cooling water flow and the water pressure in general.

As part of the testing plan, measurements of the rotor operational dynamics were made. Based on the experimentally determined frequency responses at a number of fixed speeds, the first forward whirling mode frequencies of the rotor were identified using the approach proposed in [46]. The identified forward whirling mode frequencies are plotted with red crosses in the Campbell

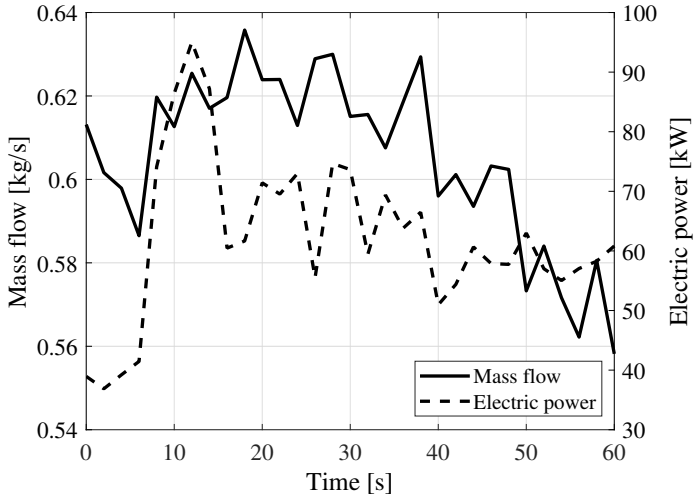

(a)

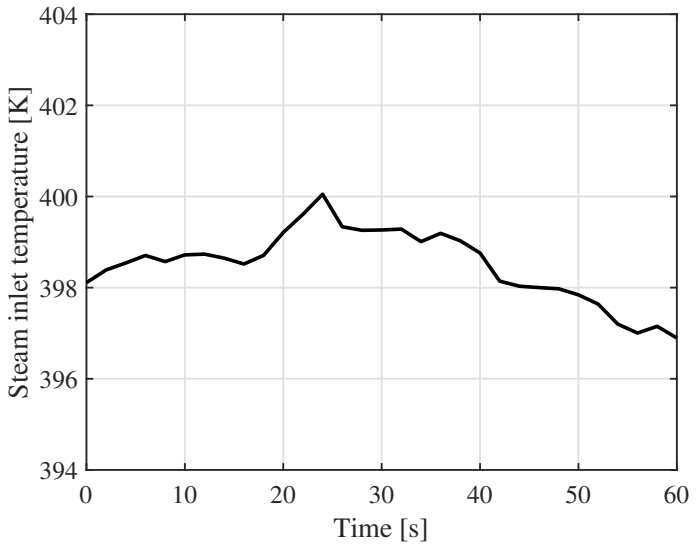

(b)

Figure 11: Turbogenerator electric power and steam mass flow (a) and inlet temperature (b) as functions of time.

diagram in Fig. 13. The figure shows a good agreement between the calculated and experimentally identified results. Furthermore, to support the design specifications for the rotor system, ramp tests were carried out to detect the possible

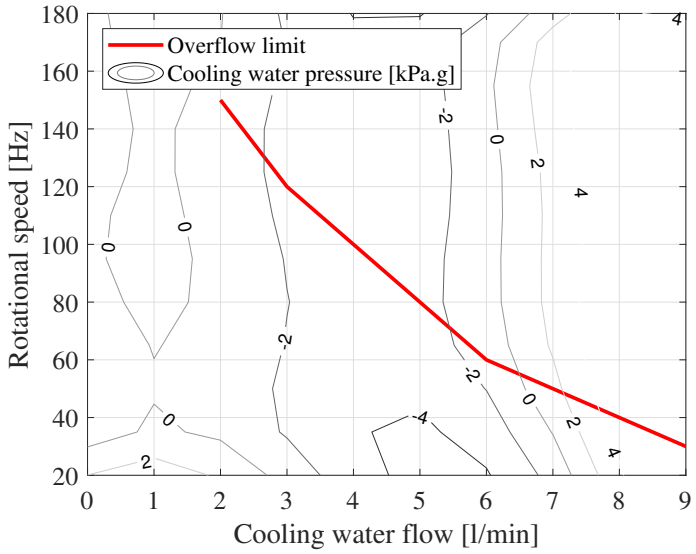

Figure 12: Effects of rotational speed and volume flow on the turbine rotor cooling water inlet pressure.

effect of unbalanced magnetic pull (UMP). The results in Fig. 14 indicate that the rotor system is well designed, as there is no harmful effect of UMP seen in the measured signals from the position sensors of the AMBs, and near the operation point, only a vibration of around 20 μm is observed. It was also observed in the tests that the coolant flow in the rotor did not reduce the rotor balance or the performance of the AMB control. Therefore, based on the design specifications, the machine operates with AMBs as expected, and it worked also under loading conditions, as was shown in Fig. 10.

6. Conclusions

This study presented a new compact hermetic high-speed radial outflow steam turbine concept that can be used in biomass and waste heat recovery applications. The study suggests that compared to conventional small-scale axial steam turbines, the ROT will have higher performance. The turbine efficiency was predicted to be 83.5%, which is comparable with the ROT performance values presented in the literature, where efficiencies above 80% are mostly re-

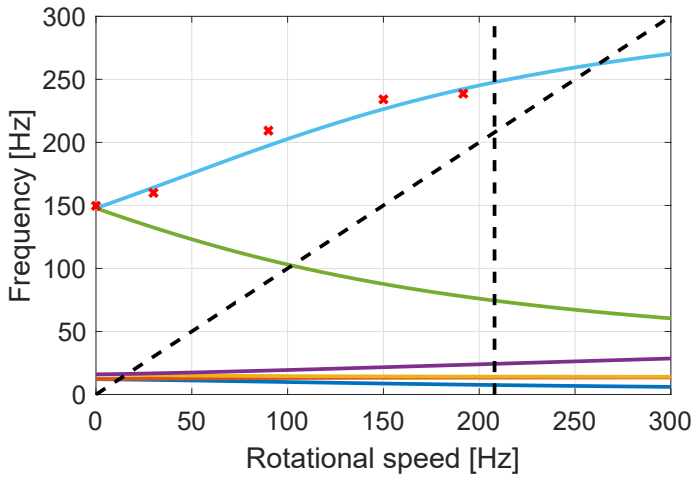

Figure 13: Campbell diagram of the turbogenerator rotor. The solid lines represent the calculated whirling mode frequencies, and the red crosses indicate the measured frequencies of the first forward whirling mode.

ported. In comparison, with typical single-stage axial turbines in conventional steam turbine designs, values even below 50% are reported.

The turbogenerator was operated under different operating conditions and it generated electricity even from very poor-quality steam. Both the rotor dynamic behavior and the performance of the magnetic bearings followed the modeled results. Therefore, it is concluded that the experiments were able to verify the turbogenerator concept. However, it is recommended that more experimental data should be made available in the future with steam values closer to the design values in order to find the limits of operation.

The effect of the rotor water cooling approach on the impeller stress distribution was studied numerically, and it was found that with the cooling, an impeller stress safety factor of 1.34 was achieved. During the experiments, the turbogenerator was operated both with and without the shaft cooling, and the cooling was found to improve the stability of the system operation. Therefore, the study was able to verify the new shaft cooling approach. In addition, the fluid dynamic behavior of the cooling was examined under different operating conditions. As a result of this analysis, an overflow phenomenon was detected

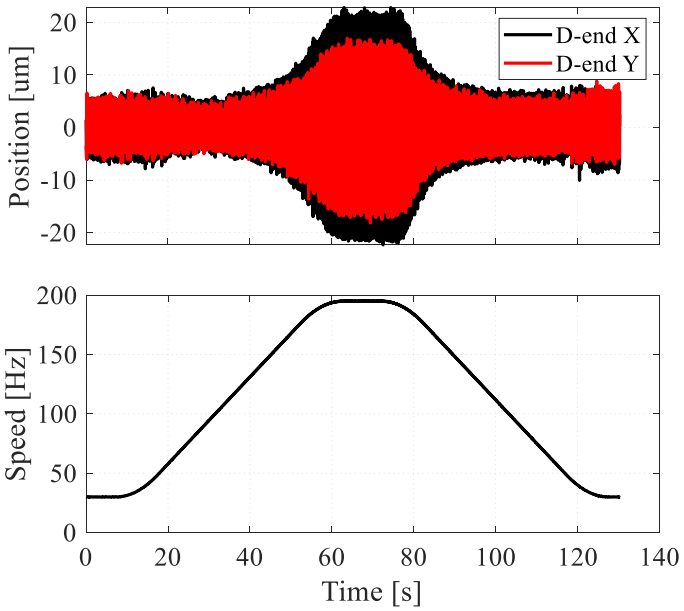

Figure 14: Validation of the rotor dynamics without load. The top graph depicts the measured position signals from the impeller-side radial AMBs when the velocity profile from 30 Hz to 195 Hz was used.

as a function of rotational speed. However, the physics behind this finding remained unsolved and a final conclusion on its causes cannot be drawn without additional research in the future.

Furthermore, the costs of the turbogenerator were found to be competitive with ORC technology and conventional steam turbines. The costs of the turbogenerator were estimated to be below 200 €/kW, while conventional steam turbines' costs are 350-636 €/kW and the lowest reported ORC project costs are 250–350 €/kW.

Acknowledgments

The research has received funding from TEKES–the Finnish Funding Agency for Technology and Innovation (nowadays Business Finland) under the grant 2748/31/2013 and from the South Carelian Regional Fund under the grant

AIKOKASVU EK15. The authors also wish to thank Professor Emeritus Jaakko Larjola for his valuable contributions at the beginning of the project.

References

[1] U. Larsen, O. Sigthorsson, F. Haglind, A comparison of advanced heat recovery power cycles in a combined cycle for large ships, Energy 74 (2014) 260–268.

[2] G. A. Livanos, G. Theotokatos, D.-N. Pagonis, Techno-Economic Investigation of Alternative Propulsion Plants for Ferries and RoRo ships, Energy Conversion and Management 79 (2014) 640–651.

[3] A. Uusitalo, J. Nerg, A. Grönman, S. Nikkanen, M. Elg, Numerical Analysis on Utilizing Excess Steam for Electricity Production in Cruise Ships, Journal of Cleaner Production 209 (2019) 424–438.

[4] S. Lion, I. Vlaskos, R. Taccani, A review of emissions reduction technologies for low and medium speed marine Diesel engines and their potential for waste heat recovery, Energy Conversion and Management 207 (2020) 112553.

[5] M. Leino, V. Uusitalo, A. Grönman, J. Nerg, M. Horttanainen, R. Soukka, J. Pyrhönen, Economics and Greenhouse Gas Balance of Distributed Electricity Production at Sawmills Using Hermetic Turbogenerator, Renewable Energy 88 (2016) 102–111.

[6] Z. Ghaffarpour, M. Mahmoudi, A. H. Mosaffa, L. Garousi Farshi, Thermoeconomic assessment of a novel integrated biomass based power generation system including gas turbine cycle, solid oxide fuel cell and Rankine cycle, Energy Conversion and Management 161 (2018) 1–12.

[7] P. Colonna, E. Casati, C. Trapp, T. Mathijssen, J. Larjola, T. Turunen-Saaresti, A. Uusitalo, Organic rankine cycle power systems: From the con-

cept to current technology, applications, and outlook to the future, Journal of Engineering for Gas Turbines and Power 137 (2015) 100801.

[8] MHI, Steam turbine generators (AT-Type), https://www.mhi-mme.com/products/boilerturbine/steam_turbine.html, Accessed 20.8.2020.

[9] Siemens steam turbine portfolio, Tech. rep., 2019.

[10] G. Persico, P. Pini, V. Dossena, P. Gaetani, Aerodynamic design and analysis of centrifugal turbine cascades, in: Proceedings of ASME Turbo Expo, June 3-7, 2013, San Antonio, Texas, USA, GT2013-95770.

[11] D. Luo, X. Tan, D. Huang, Design and Performance Analysis of Three Stage Centrifugal Turbine, Applied Thermal Engineering 138 (2018) 740–749.

[12] P. Welch, P. Boyle, New Turbines to Enable Efficient Geothermal Power Plants, GRC Transactions 3 (2009) 765–772.

[13] C. Martin, T. Kolenc, Study of Advanced Radial Outflow Turbine for Solar Steam Rankine Engines, Tech. Rep. NASA-CR-159695 (1979).

[14] L. Zanellato, M. Astolfi, A. Serafino, D. Rizzi, E. Macchi, Field Performance Evaluation of Geothermal ORC Power Plants with a Focus on Radial Outflow Turbines, Renewable Energy-doi:https://doi.org/10.1016/j.renene.2018.08.068.

[15] Y. Song, X. Sun, D. Huang, Preliminary design and performance analysis of a centrifugal turbine for Organic Rankine Cycle (ORC) applications, Energy 140 (2017) 1239–1251.

[16] A. M. Al Jubori, R. K. Al-Dadah, S. Mahmoud, A. Daabo, Modelling and Parametric Analysis of Small-Scale Axial and Radial-Outflow Turbines for Organic Rankine Cycle Applications, Applied Energy 190 (2017) 981–996.

[17] D. Di Battista, F. Fatigati, R. Carapellucci, R. Cipollone, Inverted Brayton Cycle for Waste Heat Recovery in Reciprocating Internal Combustion Engines, Applied Energy 253 (2019) 113565.

[18] A. Grönman, P. Sallinen, J. Honkatukia, J. Backman, A. Uusitalo, Design and Experiments of Two-Stage Intercooled Electrically Assisted Turbocharger, Energy Conversion and Management 111 (2016) 115–124.

[19] E. Zhao, D. Winward, Z. Yang, R. Stobart, T. Steffen, Characterisation, Control, and Energy Management of Electrified Turbocharged Diesel Engines, Energy Conversion and Management 135 (2017) 416–433.

[20] M. Renzi, F. Caresana, L. Pelagalli, G. Comodi, Enhancing Micro Gas Turbine Performance Through Fogging Technique: Experimental Analysis, Applied Energy 135 (2014) 165–173.

[21] G. Caposciutti, A. Paccioli, L. Ferrari, U. Desideri, Impact of Ambient Temperature on the Effectiveness of Inlet Air Cooling in a Co-Digestion Biogas Plant Equipped with a mGT, Energy Conversion and Management 226 (2020) 112874.

[22] J. Larjola, Electricity from industrial waste heat using high-speed organic Rankine cycle (ORC), International Journal of Production Economics 41 (1995) 227–235.

[23] T. Turunen-Saaresti, A. Uusitalo, J. Honkatukia, Design and testing of high temperature micro-ORC test stand using siloxane as working fluid, Journal of Physics: Conference Series 821 (2017) 012024.

[24] A. Jaatinen, A. Grönman, T. Turunen-Saaresti, P. Röyttä, Effect of vaneless diffuser width on the overall performance of a centrifugal compressor, Proceedings of the Institution of Mechanical Engineers, Part A: Journal of Power and Energy 225 (2011) 665–673.

[25] N. Uzhegov, A. Smirnov, C. H. Park, J. H. Ahn, J. Heikkinen, J. Pyrhönen, Design aspects of high-speed electrical machines with active magnetic bear-

ings for compressor applications, IEEE Transactions on Industrial Electronics 64 (11) (2017) 8427–8436.

[26] A. Smirnov, N. Uzhegov, T. Sillanpää, J. Pyrhönen, O. Pyrhönen, High-speed electrical machine with active magnetic bearing system optimization, IEEE Transactions on Industrial Electronics 64 (12) (2017) 9876–9885.

[27] Y. Chung, M. S. Kim, Thermal analysis and pack level design of battery thermal management system with liquid cooling for electric vehicles, Energy Conversion and Management 196 (2019) 105–116.

[28] W. Gerstler, E. Ruggiero, F. Ghasripoor, A. El-Refaie, H. De Bock, X. Shen, J. Alexander, A liquid-cooled rotor for high density electric machines, 47th AIAA/ASME/SAE/ASEE Joint Propulsion Conference & Exhibit (2011) 1–10doi:10.2514/6.2011-5560.

[29] A. Ahnger, ECC with internal combustion engines, Wärtsilä Technical Journal 2 (2007) 4–6.

[30] MAN, Waste Heat Recovery Systems (WHRS) for Reduction of Fuel Consumption, Emissions and EEDI, Tech. rep., MAN Diesel and Turbo.

[31] O. E. Balje, A study on design criteria and matching of turbomachines: Part a, similarity relations and design criteria of turbines, Journal of Engineering for Power 84 (1960) 83–102.

[32] A. H. Stenning, Design of turbines for high energy fuel, low power output applications, D.a.c.l. report 79, Massachusetts Institute of Technology (1953).

[33] A. Grönman, A. Uusitalo, J. Backman, Loss generation in radial outflow steam turbine cascades, in: Proceedings of 12th European Conference on Turbomachinery Fluid Dynamics and Thermodynamics, April 3-7, 2017, Stockholm, Sweden, ETC2017-039, pp. 1–11.

[34] M. Pini, G. Persico, E. Casati, V. Dossena, Preliminary design of a centrifugal turbine for organic rankine cycle applications, Journal of Engineering for Gas Turbines and Power 135 (2013) 042312.

[35] D. Gerada, D. Borg-Bartolo, A. Mebarki, C. Micallef, N. L. Brown, C. Gerada, Electrical machines for high speed applications with a wide constant-power region requirement, in: 2011 International Conference on Electrical Machines and Systems, 2011, pp. 1–6.

[36] N. Uzhegov, A. Pihlajamäki, J. Nerg, J. Pyrhönen, Magnetic wedges in a steam-resistant electrical machine insulation system, IEEE Transactions on Dielectrics and Electrical Insulation 22 (2015) 3153–3162.

[37] A. J. Grobler, S. R. Holm, G. van Schoor, A two-dimensional analytic thermal model for a high-speed pmsm magnet, IEEE Transactions on Industrial Electronics 62 (11) (2015) 6756–6764.

[38] J. Pyrhönen, T. Jokinen, V. Hrabovcová, Design of Rotating Electrical Machines Second Edition, John Wiley & Sons, Ltd, 2014.

[39] J. Pyrhönen, J. Nerg, P. Kurronen, U. Lauber, High-speed, 8 mw, solid-rotor induction motor for gas compression, in: 18th International Conference on Electrical Machines (ICEM), 2008, pp. 1 – 6. doi:10.1109/ICELMACH.2008.4799819.

[40] L. Bakay, M. Dubois, P. Viarouge, J. Ruel, Losses in an optimized 8-pole radial amb for long term flywheel energy storage, in: 2009 International Conference on Electrical Machines and Systems, 2009, pp. 1–6.

[41] ISO 14839-3:2004(E), Mechanical vibration – Vibration of rotating machinery equipped with active magnetic bearings – Part 3: Evaluation of stability margin, Standard, International Organization for Standardization, Geneva, CH (mar 2004).

[42] A. Filatov, L. Hawkins, Comparative study of axial/radial magnetic bearing arrangements for turbocompressor applications, Proceedings of the In-

stitution of Mechanical Engineers, Part I: Journal of Systems and Control Engineering 230 (4) (2016) 300–310. doi:10.1177/0959651815593649.

[43] S. Lemmens, Cost engineering techniques and their applicability for cost estimation of organic rankine cycle systems, Energies 9 (2016) 485.

[44] A. Arsalis, Thermoeconomic modeling and parametric study of hybrid SOFC-gas turbine-steam turbine power plants ranging from 1.5 to 10 MWe, Journal of Power Sources 181 (2008) 313–326.

[45] M. A. Ehyaei, M. A. Rosen, Optimization of a triple cycle based on a solid oxide fuel cell and gas and steam cycles with a multiobjective genetic algorithm and energy, exergy and economic analyses, Energy Conversion and Management 180 (2019) 689–708.

[46] N. Nevaranta, J. Vuojolainen, T. Sillanpää, O. Pyrhönen, Pseudo random binary signal for MIMO frequency response identification of a magnetically levitated rotor system, IOP Conference Series: Materials Science and Engineering 643 (2019) 012146. doi:10.1088/1757-899x/643/1/012146.